T2R2 東京工業大学リサーチリポジトリ
Tokyo Tech Research Repository

論文 / 著書情報
Article / Book Information

Title	Crystal structure and physical properties of new transition metal based pnictide compounds: LaTM₂AsN (TM = Fe, Co, and Ni)
Authors	Sehoon Jeong, Satoru Matsuishi, Joonho Bang, Hideo Hosono
Citation	APL Materials, Vol. 3, issue4, p. 041509
Pub. date	2015, 2
Creative Commons	See next page.

Powered by T2R2 (Tokyo Institute Research Repository)

License

Creative Commons : CC BY

Crystal structure and physical properties of new transition metal based pnictide compounds: $LaTM_2AsN$ (TM = Fe, Co, and Ni)

Sehoon Jeong, Satoru Matsuishi, Joonho Bang, and Hideo Hosono

Citation: APL Mater. **3**, 041509 (2015); doi: 10.1063/1.4913395
View online: http://dx.doi.org/10.1063/1.4913395
View Table of Contents: http://aip.scitation.org/toc/apm/3/4
Published by the American Institute of Physics

Crystal structure and physical properties of new transition metal based pnictide compounds: LaTM_2AsN (TM = Fe, Co, and Ni)

Sehoon Jeong,[1] Satoru Matsuishi,[2] Joonho Bang,[1] and Hideo Hosono[1,2]
[1]*Materials and Structures Laboratory, Tokyo Institute of Technology, 4259 Nagatsuta-cho, Midori-ku, Yokohama, Japan*
[2]*Materials Research Center for Element Strategy, Tokyo Institute of Technology, 4259 Nagatsuta-cho, Midori-ku, Yokohama, Japan*

(Received 23 December 2014; accepted 11 February 2015; published online 24 February 2015)

New 3*d* transition metal-based mixed-pnictide compounds, LaTM_2AsN (TM = Fe, Co, and Ni) are synthesized by solid state reactions under a high pressure of 2.5 GPa. These compounds crystallize with an orthorhombic structure (space group *C*mcm) containing four formula units per unit cell. The crystal structure consists of an anisotropic network of TMAs$_3$N tetrahedra sharing As-As edges along the in-plane *ac* direction and N corners along the *b*-direction, forming a TM honeycomb lattice with a boat-shape conformation bridged by TM-N-TM linear bonds. The temperature dependences of the electrical resistivity and magnetic susceptibility indicate that these crystals are itinerant antiferromagnets exhibiting parasitic ferromagnetism with transition temperatures of 560, 260, and 410 K for TM = Fe, Co, and Ni, respectively. These compounds are expected to be parent materials for new superconductors. © *2015 Author(s). All article content, except where otherwise noted, is licensed under a Creative Commons Attribution 3.0 Unported License.* [http://dx.doi.org/10.1063/1.4913395]

Since the discovery of superconductivity at T_c = 26 K in the Fe-based quaternary compound LaFeAsO,[1] FeAs-based systems have attracted a great deal of research interest toward new high-temperature superconductors (HTS). Until now, various types of Fe-based superconductors (FeSCs) have been reported and are actively being studied to understand the pairing mechanism.[2–4] The major series of FeSCs such as 1111-type *Ln*FeAsO (*Ln* = lanthanide) and 122-type *Ae*Fe$_2$As$_2$ (*Ae* = alkaline-earth) contain FeAs layers composed of edge-shared FeAs$_4$ tetrahedra which form 2-dimensional Fe^{2+} ion square lattices that possess metallic conductivity with stipe-type antiferromagnetic (AFM) ordering of the Fe spins.[5–7] The superconductivity is induced by carrier (electron or hole) doping into the FeAs-layer to suppress the AFM ordering.[8–10] Therefore, transition metal pnictides composed of edge-shared $TMPn_4$ (TM = transition metal; Pn = pnictgen) tetrahedra, especially those that exhibit magnetic ordering, have been investigated to find new parent HTS compounds.[11–13] In addition to Fe site substitution, replacing the As sites has been examined. Generally, fully P-substituted Fe-based compounds are paramagnetic at a normal conducting state and their T_c values are lower than 10 K.[14] However, the superconductivity is induced as well by partial P-substitution of Fe-based compounds.[15,16] These results imply that the interactions between the Fe 3*d* and *Pn p* orbitals play an important role in their pairing mechanism.

Here, we report new transition metal-based mixed-pnictides LaTM_2AsN (TM = Fe, Co, and Ni) that are synthesized by solid state reactions under high-pressures. The powder X-ray diffraction (PXRD) data demonstrate that these compounds consist of TMAs$_3$N tetrahedra sharing As-As edges and N corners, forming a TM honeycomb lattice with a boat-shape conformation in place of the Fe square net of FeSCs. It is revealed that each compound is an itinerant AFM magnet with a magnetic transition temperature of 260–560 K.

The polycrystalline LaTM_2AsN compounds were synthesized by the solid-state reaction of LaN and TM_2As (LaN + TM_2As → LaTM_2AsN) using a belt-type high-pressure anvil cell. The

 ©Author(s) 2015

TABLE I. The analyzed chemical compositions for LaTM_2AsN.

Compound	Molar composition (La : *TM* : As : N : O)
$LaFe_2AsN$	1.00 (2) : 2.07 (3) : 1.057 (5) : 0.90 (1) : 0.020 (1)
$LaCo_2AsN$	1.000 (6) : 2.05 (1) : 0.97 (1) : 0.83 (2) : 0.04 (1)
$LaNi_2AsN$	1.000 (7) : 1.99 (1) : 0.968 (5) : 0.71 (2) : 0.04 (2)

chemical compositions of the products were determined using an electron probe micro-analyzer (EPMA). The PXRD patterns of samples were measured using a D8 ADVANCE (Bruker AXS GmbH, Germany) with Cu Kα radiation at 300 K. The peak indexing and the Rietveld refinement of the PXRD patterns were performed using TOPAS code.[17] The temperature dependence of the DC electrical resistivity in the temperature range of 2-300 K and the magnetic susceptibilities at high temperatures of 300–750 K were measured using physical properties measurement system (PPMS; Quantum Design, USA). The magnetic susceptibilities at low temperature range of 2-400 K were measured using a superconducting quantum interference device vibrating sample magnetometer (SQUID-VSM).[18]

The results of the element composition analysis using an EPMA are summarized in Table I. It is shown in the back-scattered electron images in the supplementary material[18] (Fig. S1) that the synthesized samples were polycrystalline with the elemental composition: La:*TM*:As:N = 1:2:1:0.71-0.90. However, a small amount of secondary phases such as LaFeAsO, Co, Co_5As_2, La_2O_3, and $LaNi_5As_3$ were segregated at the grain boundaries. Upon taking account of the low X-ray fluorescence generation efficiency of nitrogen, the actual chemical formula of the main phases is closer to LaTM_2AsN.

Figure 1 shows the PXRD pattern for the $LaFe_2AsN$ sample. First, we tried to determine the crystal structure by indexing the reflections.[18] As a result of the Rietveld refinement using the above constraints, we succeed in fitting the PXRD patterns. The refinement results for the powder XRD patterns for $LaCo_2AsN$ and $LaNi_2AsN$ are also shown in Fig. S2 in the supplementary material.[18] These refinements were performed using a structure model with crystallographic parameters and atomic positions (see Table II). The atomic bonding nature is summarized in Table SI in the supplementary material.[18]

Figure 2(a) shows the structural model for LaTM_2AsN. The *TM* sites ($8f$; (x, y, z) = (0, y_{TM}, z_{TM})) were coordinated by three As sites ($4c$; (0, y_{As}, 1/4)) and one N site ($4a$; (0, 0, 0)), forming an anisotropic network of $TMAs_3N$ tetrahedra that share As-As edges along the in-plane *ac* direction and N corners along the *b*-direction. Figure 2(b) is a close-up view of adjacent $TMAs_3N$ tetrahedra sharing As-As edge along *a* direction. Each tetrahedron has C_s point group symmetry with a mirror plane perpendicular to *a* direction containing *TM*, N, and one of the three As sites. Thus, there are two types of *TM*-As bonds (0.2477 and 0.2467 nm for *TM* = Fe) with one *TM*-N

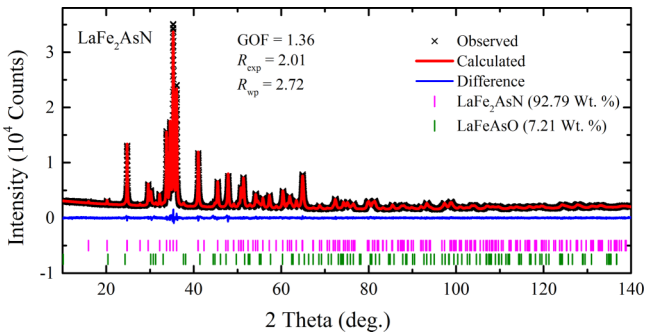

FIG. 1. PXRD pattern (crosses) and calculated curves (solid red line) based on the Rietveld refinement of $LaFe_2AsN$ at room temperature. The blue solid line is the difference between the observed and calculated intensities. The pink and green vertical bars indicate the calculated Bragg diffraction positions for $LaFe_2AsN$ and LaFeAsO, respectively.

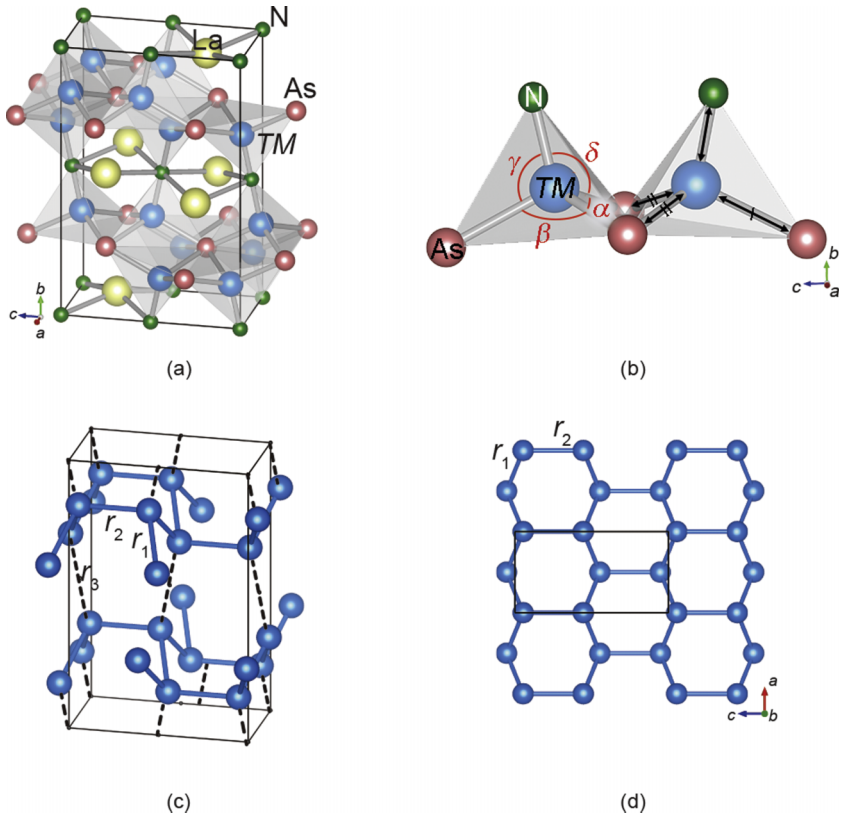

FIG. 2. (a) Crystal structure of LaTM_2AsN. The solid lines show the unit cells. (b) Close-up view of adjacent TM_3AsN tetrahedra. (c) and (d) depict the *TM* honeycomb lattice with a boat conformation. r_i (where i = 1, 2, and 3) indicates the i-th neighboring *TM*-*TM* separations. The yellow, blue, pink, and green spheres represent La, *TM*, As, and N atoms, respectively.

bond (0.188 nm for *TM* = Fe) tilted from *b* direction. Due to the mirror plane perpendicular to *c* direction, the direction of *TM*-N bond in the adjacent tetrahedra is anticlinal to each other and there is no inversion symmetry. Figures 2(c) and 2(d) show the network structure of neighboring *TM* sites forming honeycomb lattice with a boat-shape conformation. The first and second neighboring Fe-Fe separations are 0.278 and 0.282 nm, which are comparable to the first neighboring distance in FeSCs (0.284 nm for LaFeAsO and 0.280 nm for $BaFe_2As_2$).[19,20]

Figure 3 shows the temperature dependence of the electrical resistivity in LaTM_2AsN. All of the compounds show the positive temperature dependences with room temperature resistivities of

TABLE II. The refined crystallographic parameters and atomic positions for LaTM_2AsN.

	$LaFe_2AsN$	$LaCo_2AsN$	$LaNi_2AsN$
Lattice constant			
a (nm)	0.379932 (3)	0.375993 (5)	0.371584 (5)
b (nm)	1.111461 (8)	1.11674 (1)	1.14147 (1)
c (nm)	0.718656 (6)	0.70185 (1)	0.69786 (1)
V (nm^3)	0.303474 (4)	0.294699 (7)	0.296004 (7)
Atomic position			
y_{TM}	0.16531 (7)	0.1651 (1)	0.1685 (1)
z_{TM}	0.0540 (1)	0.0535 (2)	0.0530 (2)
y_{As}	0.73132 (7)	0.7307 (1)	0.7320 (1)
y_{La}	0.45717 (4)	0.45790 (7)	0.46067 (7)

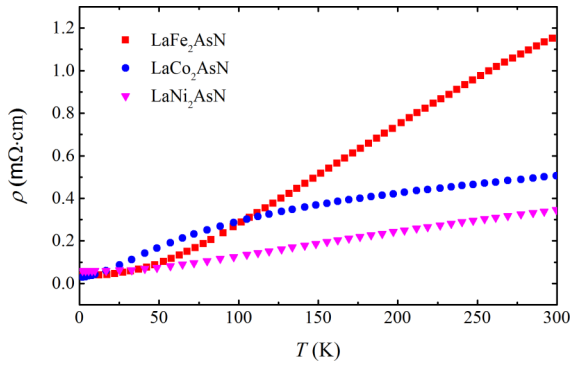

FIG. 3. Temperature dependence of the electrical resistivity (ρ) for LaTM_2AsN.

1.16, 0.51, and 0.35 mΩ cm for *TM* = Fe, Co, and Ni, respectively. These values are comparable to that of LaFeAsO[21] and indicate that the edge-shared MAs$_3$N structure is metallic in nature, similar to La*TM*AsO compounds.[1,22] In case of *TM* = Fe and Ni, the temperature dependence of resistivity could be fitted by Bloch-Grüneisen theory (BG theory) with the value of exponent $n \approx 3$ (see Fig. S3 of supplementary material[18]). It is indicated that the resistivity observed is due to *s*-*d* electron scattering from Fe or Ni. However, the data of $LaCo_2AsN$ showing a downward curvature could not be explained by BG theory in range of 50-300 K but could be fitted with $n \approx 2$ in the range of 2-50 K. The downward curvature for $LaCo_2AsN$ is likely to originate from secondary phase of ferromagnetic Co metal (2.53 wt. % or 13.2 mol. %) which shows similar temperature dependence.[23]

Figures 4(a)-4(c) show the high-temperature zero-field cooled (ZFC) and field cooled (FC) magnetic susceptibilities (χ) of LaTM_2AsN measured at a magnetic field of 200 Oe. The magnetic susceptibilities of these compounds were <1.03 emu/mol *TM* above 600 K. A sharp rise in the FC susceptibility was observed at 560 K for *TM* = Fe and 410 K for *TM* = Ni. Figures 4(d)-4(f) show the ZFC and FC χ-T curves in the low temperature range. For *TM* = Co, a similar increase in the FC susceptibility was observed at 260 K. While a monotonic increase in the FC susceptibility is

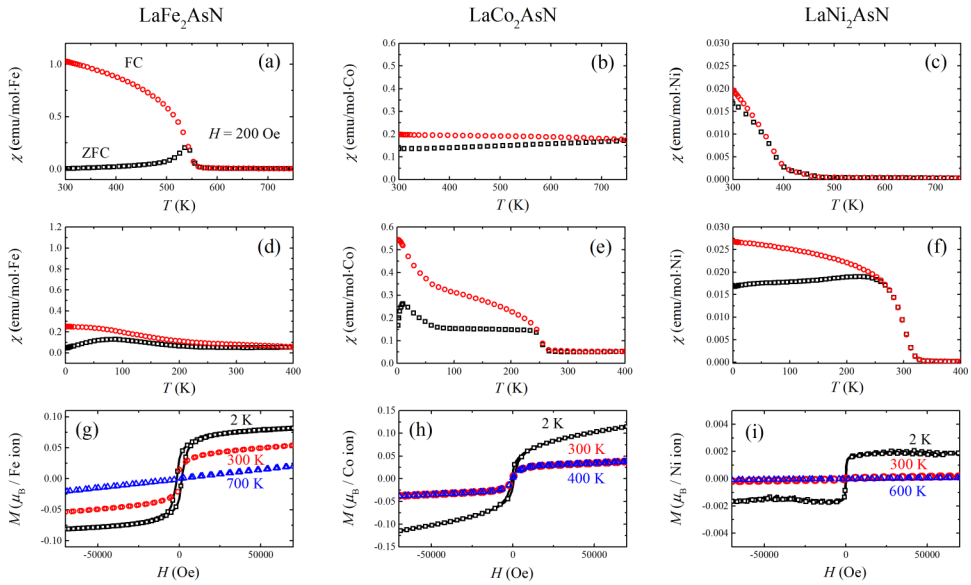

FIG. 4. Temperature dependence of the susceptibility and field dependence of the magnetization for $LaFe_2AsN$ in (a), (d), (g), $LaCo_2AsN$ in (b), (e), (h), and $LaNi_2AsN$ in (c), (f), (i), measured from 1.8 K to 400 K using SQUID, and from 300 K to 750 K using a VSM. Please note that the vertical scales are different for each graph.

typical in ferromagnetic (FM) states, the peak and shoulders in the ZFC curves are typical in AFM states, indicating that AFM and FM transitions simultaneously occurred just below the magnetic transition temperature T_M of 560, 260, and 410 K for *TM* = Fe, Co, and Ni, respectively. Since none of secondary phases detected by EPMA has magnetic transition around the T_M, the observed rises of susceptibility are attributed to the main phases (see Table S1 of supplementary material[18]). The coexistence of AFM and FM states is also confirmed by non-linearity of $1/\chi$ *vs*. T plot above T_M (see Fig. S4 of supplementary material[18]). Figures 4(g)-4(i) show the magnetization (M) *vs*. magnetic field (H) curves observed at 2 K, 300 K, and temperatures above T_M (700, 400, and 600 K). The M-H curves at 2 K show the FM behavior with small magnetic moments at 70 kOe corresponding to 0.08, 0.1, and 0.002 μ_B/TM for *TM* = Fe, Co, and Ni, respectively. The preliminary result of neutron powder diffraction (NPD) study at 300 K demonstrated that $LaFe_2AsN$ is antiferromagnet with stripe-type order of Fe spins with a local moment of 1.70 (1) μ_B along b direction. In this AFM state, the local moments of adjacent Fe sites shown in Fig. 2(b) have opposite directions. Details of NPD data analysis will be published in a separate paper. Generally, the coexistence of weak FM and AFM order could be explained by ferri-magnetism, spin-glass, and canted-AFM or delocalized FM (+AFM) moment. The result of NPD indicates that the canted-AFM and delocalized FM moment are the possible origins of the observed weak FM. Here, we notice that the absence of inversion symmetry between neighboring *TM* sites in LaTM_2AsN is favorable to realize canted-AFM state. If the observed weak FM orignates from the spin-canting, the effective magnetic moment should increase with magnetic field as shown in M-H curves, because the spin canting angle can be easily changed along a magnetic easy axis. In addition, the increase of the FC susceptibility and the presence of a peak in the ZFC curve at low temperature (< ~80 K for *TM* = Fe and Co) can be explained by the re-orientation of the spin canting direction.

For *TM* = Fe and Ni, the high temperature M-H curves above T_M were almost linear, corresponding to the paramagnetic state with small magnetic moment at 70 kOe of 0.02, and 0.000 08 μ_B/TM, respectively. Such a small magnetic moment is likely to originate from the coexistence of itinerant and localized electrons in these compounds. For *TM* = Co, the M-H curve shows the saturating behavior with small magnetic moments of 0.04 μ_B/Co at 70 kOe even above T_M. This small FM moment comes from segregated Co with T_C = 1404 K.

In summary, the new compounds of 3d transition-metal based mixed-pnictides, LaTM_2AsN (*TM* = Fe, Co, and Ni) have been identified as orthorhombic crystals (space group *C*mcm) by complementary analysis using EPMA and X-ray Rietveld refinement. These compounds are composed of an anisotropic $TMAs_3N$ tetrahedra network parallel to the [010] plane with a *TM* honeycomb lattice arranged in a boat-shape conformation. The electrical resistivity and magnetic susceptibility data indicated that there was an itinerant AFM state combined with a weak ferromagnetic component. The itinerant AFM behavior, similar to LaFeAsO, implied that the LaTM_2AsN compound is a candidate of parent compound for superconductors.

This work was supported by the MEXT Elements Strategy Initiative to Form Core Research Center "Tokodai Institute for Element Strategy (TIES)."

[1] Y. Kamihara, T. Watanabe, M. Hirano, and H. Hosono, J. Am. Chem. Soc. **130**, 3296 (2008).
[2] K. Ishida, Y. Nakai, and H. Hosono, J. Phys. Soc. Jpn. **78**, 062001 (2009).
[3] J. Paglione and R. L. Greene, Nat. Phys. **6**, 645 (2010).
[4] W. Wang, B. Li, S. Liu, M. Liu, and Z. W. Xing, J. Appl. Phys. **107**, 123906 (2010).
[5] C. de la Cruz *et al.*, Nature **453**, 899 (2008).
[6] J. Guo, S. Jin, G. Wang, S. Wang, K. Zhu, T. Zhou, M. He, and X. Chen, Phys. Rev. B **82**, 180520 (2010).
[7] T. Nomura, S. W. Kim, Y. Kamihara, M. Hirano, P. V. Sushko, K. Kato, M. Takata, A. L. Shluger, and H. Hosono, Supercond. Sci. Technol. **21**, 125028 (2008).
[8] H. Luetkens *et al.*, Nat. Mater. **8**, 305 (2009).
[9] S. Matsuishi, Y. Inoue, T. Nomura, H. Yanagi, M. Hirano, and H. Hosono, J. Am. Chem. Soc. **130**, 14428 (2008).
[10] A. S. Sefat, A. Huq, M. A. McGuire, R. Jin, B. C. Sales, D. Mandrus, L. M. Cranswick, P. W. Stephens, and K. H. Stone, Phys. Rev. B **78**, 104505 (2008).
[11] Q. Huang, Y. Qiu, W. Bao, M. Green, J. Lynn, Y. Gasparovic, T. Wu, G. Wu, and X. Chen, Phys. Rev. Lett. **101**, 257003 (2008).
[12] X. W. Yan, M. Gao, Z. Y. Lu, and T. Xiang, Phys. Rev. Lett. **106**, 087005 (2011).
[13] X. Zhu, F. Han, G. Mu, B. Zeng, P. Cheng, B. Shen, and H. H. Wen, Phys. Rev. B **79**, 024516 (2009).
[14] Y. Kamihara, H. Hiramatsu, M. Hirano, R. Kawamura, H. Yanagi, T. Kamiya, and H. Hosono, J. Am. Chem. Soc. **128**, 10012 (2006).

[15] M. Nakajima, S. I. Uchida, K. Kihou, C. H. Lee, A. Iyo, and H. Eisaki, J. Phys. Soc. Jpn. **81**, 104710 (2012).
[16] C. Wang *et al.*, Europhys. Lett. **86**, 47002 (2009).
[17] TOPAS, version 4.2 Bruker AXS, Karlsruhe, Germany, 2009.
[18] See supplementary material at http://dx.doi.org/10.1063/1.4913395 for the details on the sample preparation, composition analysis, X-ray diffraction, resistivity measurements and magnetic susceptibility measurements.
[19] D. Mandrus, A. S. Sefat, M. A. McGuire, and B. C. Sales, Chem. Mater. **22**, 715 (2010).
[20] I. R. Shein, A. N. Enyashin, and A. L. Ivanovskii, Comput. Mater. Sci. **50**, 824 (2011).
[21] M. McGuire *et al.*, Phys. Rev. B **78**, 094517 (2008).
[22] T. Watanabe, H. Yanagi, Y. Kamihara, T. Kamiya, M. Hirano, and H. Hosono, J. Solid State Chem. **181**, 2117 (2008).
[23] A. K. Pal, S. Chaudhuri, and A. K. Barua, J. Phys. D: Appl. Phys. **9**, 2261 (1976).